Effect of counter-phase pump modulation of phase-sensitive amplifiers noise performance and SBS suppression

Research Article Vol. 33, No. 7 / 7 Apr 2025 / Optics Express 16174
Optics EXPRESS

Effect of counter-phase pump modulation of phase-sensitive amplifiers noise performance and SBS suppression

RUWAN U. WEERASURIYA,* RASMUS LARSSON, AND PETER A. ANDREKSON

Department of Microtechnology and Nanoscience, Chalmers University of Technology, Kemivägen 9, Gothenburg 41296, Sweden
*ruwan.udayanga@chalmers.se

Abstract: Optical phase-sensitive amplifiers (PSAs) leverage nonlinear interactions to achieve noise figures below the conventional quantum limit. Dual-pump phase-insensitive amplification has been studied in wavelength conversion, phase conjugation and spectral inversion, but phase-sensitive amplification remains challenging due to stimulated Brillouin scattering (SBS) in optical fibers. While pump-phase modulation helps mitigate SBS, it broadens the idler spectrum, complicating practical implementation. We demonstrate a counter-phase pump modulation approach to suppress idler spectral broadening using optical coherent combining and delayed self-heterodyne techniques to achieve excellent noise figure (NF) performance in dual-pump PSAs. Our methods achieve over 30 dB suppression of residual phase modulation tones and significantly improve the idler spectrum. We obtained a 20 dB gain with an NF of 1.45 dB and a minimal NF penalty of 0.2 dB due to pump-phase modulation. This achievement enables PSAs to support optical communication, wavelength conversion, and deep-space communication applications.

1. Introduction

Four-wave mixing (FWM) can be excited in χ^3 media, where power from co-propagating strong pumps is transferred to a weaker signal and an idler through nonlinear interaction. The pumps, signal, and idler frequencies need to maintain a specific frequency and phase relationship during this process to be efficient. FWM is an essential method for nonlinear optical processing, wavelength conversion, format conversion, and optical parametric amplification (OPA). Among these, wavelength conversion and OPA have been of significant interest during the last decades [1,2].

Wavelength converters are vital in wavelength division multiplexing (WDM) networks, allowing flexible, non-blocking wavelength routing and management [3,4]. Most existing wavelength converters use optical-electrical-optical (OEO) techniques, providing good signal quality but lacking modulation and bit format transparency. Those OEO-based wavelength converters have major drawbacks from underlying electronics which have operating high-frequency limitations. These limitations can be overcome with all-optical wavelength converters, which have been demonstrated using various techniques [5–8]. Fibre optical parametric amplifiers (FOPAs) offer wide bandwidth [9,10] and high-gain continuous wave (CW) amplification [11,12] thus making them suitable as both amplifiers and wavelength converters.

FOPAs' ability to amplify and process optical signals in unconventional optical bands enhances optical communication, allowing operation outside standard rare-earth-doped bands and enabling multiple conventional telecommunication bands [12]. In a simple FOPA configuration, a single

#551379 https://doi.org/10.1364/OE.551379
Journal © 2025 Received 7 Dec 2024; revised 26 Feb 2025; accepted 4 Mar 2025; published 3 Apr 2025

Optics EXPRESS

pump wave and a weaker signal wave interact in a dispersion-engineered highly nonlinear fiber (HNLF), generating an idler wave through third-order nonlinearity (Kerr effect) [1,13]. A more complex dual-pump FOPA scheme can be implemented in non-degenerate (Fig. 1(a)) or degenerate configurations (Fig. 1(b)) [13]. In the non-degenerate case, the signal and idler are situated at separate frequencies between the pumps. Meanwhile, the signal coincides with the idler frequency created through FWM in the degenerate configuration. While PSAs can be implemented using both configurations, the non-degenerate case is suitable for wavelength converters and the degenerate scheme is suitable for regeneration schemes [2,13,14].

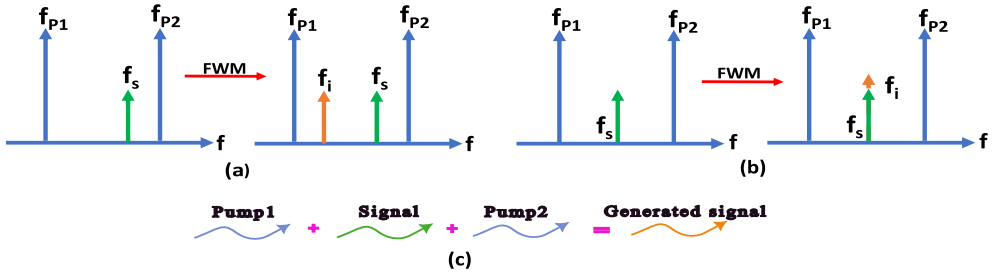

Fig. 1. Illustration of FWM-mixing for a dual-pump scenario, (a) non-degenerate signal and idler, (b) degenerate signal and idler and (c) new signal (idler) generation through FWM process. The idler power in (b) would be equal to or lower than the signal power, but for clarity, the place of the idler was shown above the signal.

FOPA performance, however, is hindered by stimulated Brillouin scattering (SBS) [1,2] which causes reflection of high pump powers, thus severely limiting the gain of the nonlinear process. Pump dithering (phase modulation), which is used to suppress the SBS by spreading the pump wave spectrum, increases the SBS threshold but simultaneously degrades the converted idler quality by broadening its spectrum [2,15]. In single- or dual-pump FOPAs, idler spectral broadening often reaches several gigaHertz when suppressing SBS, which is too large for many applications. A solution for this idler spectrum broadening was introduced in dual-pump FOPAs by out-of-phase dithering on two pumps [2,16–18]. However, residual amplitude modulation, dispersion effects, and phase and polarization fluctuations can negatively impact this technique [2,16,17] and the level of idler cleaning achieved in [2,17] was not entirely satisfactory (17 dB). This is particularly problematic in PSAs as a pure idler is very important to reach a low noise figure (NF).

Compared to other OPA techniques, such as χ^2-based parametric amplifiers and single-pump nonlinear photonic waveguide amplifiers, which inherently do not suffer from SBS [19–21], the dual-pump FOPA offers distinct advantages. These include broadband gain, tunability, and phase-sensitive amplification, making it highly suitable for applications requiring low-noise amplification and signal regeneration. Additionally, the dual-pump FOPA can provide a broader amplification bandwidth than χ^2-based systems and greater design flexibility compared to single-pump waveguide-based OPAs. Despite the need for SBS mitigation, these advantages make dual-pump FOPA a compelling choice for advanced optical communication and signal processing applications [2,11].

In this work, we propose and experimentally evaluate techniques such as coherent combining [22,23] with RF path length matching [2,22] for optimizing the opposite dithering technique. We use delayed self-heterodyne (DSHD) techniques to analyze and visualize the idler spectrum, which will address issues associated with coherent intradyne analysis [2,24]. Very little research has been conducted to extend the dual-pump FOPA to a PSA scheme. As discussed earlier, the main bottleneck is the idler containing the residual effects of pump phase modulation. To our knowledge, this is the first implementation of a dual-pump PSA scheme that employs pump phase

Optics EXPRESS

modulation using multiple RF tones to suppress SBS and uses an amplitude and phase alignment circuit to cancel out the pump phase modulation in the idler. This technique was first used in [25] to demonstrate an ultralow noise preamplified optical receiver using conventional single wavelength transmission.

In this paper, we evaluate this technique and experimentally demonstrate the amount of idler purification achieved by canceling the pump phase modulation using opposite dithering. Moreover, we evaluate and experimentally demonstrate the effect on performance versus the amount of residual phase modulation left on the idler due to pump phase modulation for the PSA preamplification. All these demonstrations and evaluations were conducted using a dual-pump degenerate scheme (Fig. 1(b). In section 2 we present the underlying methodology and theory of SBS suppression using counter-phased pumps, in section 3 the experiments and results are discussed and a conclusion is provided in section 4.

2. SBS suppression using pump-phase modulation

Since our goal is to implement a dual-pump PSA scheme in presence of SBS, we aimed to significantly increase the SBS threshold [26] through pump modulation (further discussion in Supplement 1, sect. A). By applying three sine tones centred at 95 MHz, 305 MHz, and 490 MHz to both pumps, we increased the SBS threshold from 16 dBm per pump, without phase modulation, to over 20.5 dBm, 24.4 dBm, and 28.6 dBm with one, two, and three tones, respectively, as shown in Fig. 2. Theoretical SBS threshold increase predictions are 4.8, 9.5 and 14.3 dB [26].

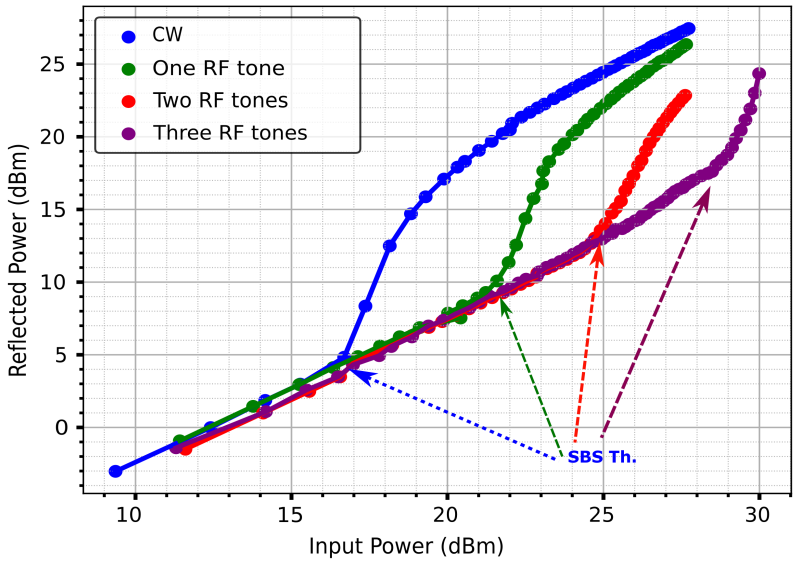

Fig. 2. SBS threshold with one (f_1), two ($f_1 + f_2$), and three ($f_1 + f_2 + f_3$) tones; $f_1 = 95$ MHz, $f_2 = 305$ MHz, $f_3 = 490$ MHz

While the phase-modulation suppressed SBS, the idler spectral broadening it causes limits the implementation of wavelength converters (WCs) or PSAs. Therefore, it is crucial to analyze the impact of pump dithering on idler broadening. This analysis discusses the effect considering the dual-pump non-degenerate signal and idler scenario where we can physically identify the idler. Although this model is discussed for the non-degenerate case, it also applies to the degenerate scenario.

Optics EXPRESS

Let us first consider the dual-pump non-degenerate signal-idler configuration (Fig. 1(a)). The generated idler frequency and phase relationship are provided by

$$\omega_i = \omega_{p1} + \omega_{p2} - \omega_s, \quad \phi_i = \phi_{p1} + \phi_{p2} - \phi_s \tag{1}$$

where, ω_i, ϕ_i, ω_{p1}, ϕ_{p1}, ω_{p2}, ϕ_{p2}, ω_s, and ϕ_s are the angular frequency and the phase of idler, pump 1, pump 2 and signal, respectively.

The same relationship also holds for the degenerate case ($\omega_s = \omega_i$, $\phi_s = \phi_i$) where single wavelength amplification and regeneration were demonstrated [14]. Let us examine the case where the two pumps are phase-modulated by one RF tone. If we assume the phase modulation of the two pumps has different magnitudes and phases which arise due to different RF component and path length mismatches at the modulator input for each pump, the pump phases after modulation can be expressed by

$$\phi_{p1}(t) = \omega_{p1}t + \phi_{m1}\cos(\omega_m t), \quad \phi_{p2}(t) = \omega_{p2}t + \phi_{m2}\cos(\omega_m(t+\tau)) \tag{2}$$

where ϕ_{m1} and ϕ_{m2} are the dither magnitudes of the RF tone m at pump 1 and 2, respectively, ω_m is the frequency of the RF tone and τ is the relative time delay of the applied RF tone between the two pumps.

By considering Eqs. (1) and (2), we can further extend the idler phase as

$$\phi_i = [\omega_{p1}t + \phi_{m1}\cos(\omega_m t)] + [\omega_{p2}t + \phi_{m2}\cos(\omega_m(t+\tau))] - \phi_s \tag{3}$$

and, with further simplification, we can separate the continuous-wave (CW)-related ($\phi_{i,\mathrm{cw}}$) and phase-modulated related components ($\phi_{i,\mathrm{mod}}$) as

$$\phi_i = \phi_{i,\mathrm{cw}} + \phi_{i,\mathrm{mod}}, \quad \phi_{i,\mathrm{cw}} = \omega_{p1}t + \omega_{p2}t - \phi_s, \quad \phi_{i,\mathrm{mod}} = \phi_{m1}\cos(\omega_m t) + \phi_{m2}\cos(\omega_m(t+\tau)) \tag{4}$$

The phase modulation component ($\phi_{i,\mathrm{mod}}$) must be zero to eliminate the effects of pump phase modulation on the idler. Using this reasoning, we can demonstrate that the net phase difference between the modulating signals at the two modulators, or the FOPA, must be an odd multiple of π and the magnitudes must be equal $\phi_{m1} = \phi_{m2}$. In case of multiple tones, these requirements apply to each applied RF tone. It becomes evident that the two modulating signals should be out of phase with each other, either leading or lagging by a phase shift of π. This conclusion is also confirmed by Eq. (11) in [17].

To minimize the residual pump phase modulation on the idler ($\phi_{i,\mathrm{mod}}$) in a practical system, we characterize the voltage to phase transfer function (from non-ideal components) $\phi_{pi} = H_i(V_{m,i}, f_m) \cdot V_{m,i}$ for each pump $i = 1, 2$ and RF tone $m = 1, 2, 3$. When combined with individual control of magnitude and delay for each RF tone, the transfer function provides a simple and direct way of calculating and creating the appropriate analog dither signals, e.g., using an arbitrary waveform generator (AWG), as in our case. To find the transfer magnitude $|H_i|$ we utilized the coherent combining technique [22,23], illustrated in Fig. 3(a). For matching the final delays in the actual PSA, the setup in Fig. 3(b) was used, which is the same as would be used for phase-sensitive amplification or wavelength conversion. In both cases shown in Fig. 3(a) and (b), a separate 35 MHz dither signal was introduced to assist in tracking phase mismatch and optimizing the optical phase-locked loop (OPLL) [27].

2.1. Transfer magnitude characterization

In the configuration of Fig. 3(a), the output power of the second 3dB coupler is proportional to the locking efficiency, or combining efficiency [23]

$$\eta = \frac{1}{2}[1 + \cos\phi_{i,\mathrm{mod}}] \tag{5}$$

for the arm with constructive interference and $\propto 1 - \eta$ for the destructive arm. Here we assume that any residual phase error from the PLL is negligible by ensuring the phase variation is within

Optics EXPRESS

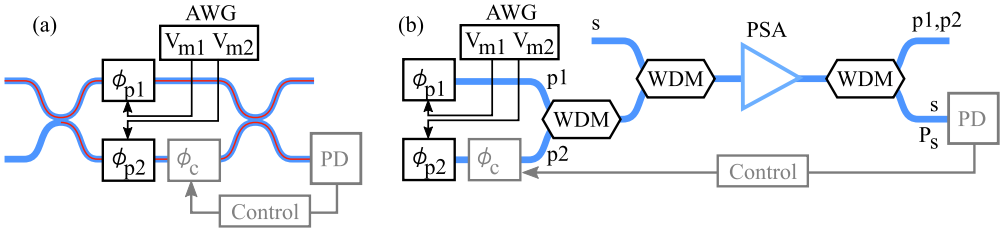

Fig. 3. (a) The coherent combining setup. A CW laser is split using a 3dB coupler and is sent through each pump-phase modulator before being recombined in a secondary 3 dB coupler with equal power at both inputs. An AWG is used to generate the RF tones with voltage magnitudes $V_{m,i}$. The shaded section represents a slow phase-locked loop (PLL) which actively compensates natural phase fluctuations between the two arms and coherently combines the power on either output port. (b) Similar to (a) but with constructive interference between pumps and signal in a PSA instead of a 3dB coupler. Polarization controllers were used in both setups to align the waves at all points.

the PLL bandwidth and that the OPLL control signal has high SNR. The locking efficiency is used to characterize H but also provides an estimate of the impact of residual pump-phase dithering.

By measuring the power ratio between constructive and destructive ports, i.e. the extinction ratio $\mathrm{ER} = \eta/(1-\eta)$ (can be done from the same port by switching which arm is construcive/destructive using the PLL), the locking efficiency can be estimated as

$$\eta = \frac{\mathrm{ER}}{1+\mathrm{ER}}, \quad \langle\eta\rangle \approx \frac{\langle \mathrm{ER}\rangle}{1+\langle \mathrm{ER}\rangle}, \tag{6}$$

where $\langle\cdot\rangle$ represents the time-average estimate (which is simply obtained using a power meter). Time-averaging smooths out the rapid oscillations introduced by the dither (ϕ_c). As a result, the $\langle\eta\rangle$ or $\langle ER\rangle$ appears as a stable, averaged value that reflects the overall performance.

Rewriting Eq. (4) with $\tau = \pi/\omega_m + \tau_e$, where τ_e is a delay-mismatch which may persist due to small path mismatches even at the near-optimal pump phase alignment achieved through the AWG, we have

$$\phi_{i,\mathrm{mod}} = \Phi_{m1}\cos\omega_m t + \Phi_{m2}\sin\omega_m t, \quad \Phi_{m1} = \phi_{m1} - \phi_{m2}\cos\omega_m\tau_e, \quad \Phi_{m2} = \phi_{m2}\sin\omega_m\tau_e \tag{7}$$

which we use to write the time-average locking efficiency (refer to section 1.D in Supplement 1 text for derivation)

$$\langle\eta\rangle = \frac{1}{2}\left[1 + \prod_{m=1}^{N} J_0\left(\sqrt{\Phi_{m1}^2 + \Phi_{m2}^2}\right)\right] \approx \frac{1}{2}[1+\exp(-\Delta\phi^2/4)], \quad \Delta\phi^2 = \sum_{m=1}^{N}\Phi_{m1}^2 + \Phi_{m2}^2 \tag{8}$$

where N is the number of applied RF tones and J_0 is the Bessel function of the first kind.

If only one RF tone is applied to one modulator with voltage $V_{m,i}$ the argument of $J_0(x)$ reduces to ϕ_{mi} (irrespective of delay τ_e). The measured extinction ratio for the applied voltage $V_{m,i}$ can then be used to calculate the corresponding phase ϕ_{mi} via $\langle\eta\rangle$ from which $|H_i(V_{m,i},f_m)| = \phi_{mi}/V_{m,i}$ is found. For high accuracy one preferably characterizes $|H|$ for a $V_{m,i}$ that results in a low $|\langle\eta\rangle|$ (where $|d/dx(J_0(x))|$ is large). This process can then be repeated to characterize the transfer for each RF tone in each modulator. With the knowledge of the transfer for each tone, it is straightforward to obtain matched phase modulation between modulators and equal phase-modulation depth for each tone, by simply setting the input voltage $V_{m,i} = V_0/|H_i(V_{m,i},f_m)|$ where V_0 is a single parameter with which the total modulation strength can be tuned.

Optics EXPRESS

2.2. Delay optimization

Delay optimization in its simplest form can be carried out changing the length of either the optical propagation after each modulation or the RF-length before the modulator for one pump, in relation to the other pump. This approach does not allow delay adjustments between each RF tone which is necessary to combat the frequency-dependent transfer $H_i(V_{m,i},f_m)$. The AWG is convenient in this aspect as an individual delay is easy to control digitally. For the initial optimization of the delay, we used the coherent combining setup once more, now enabling one RF tone at a time simultaneously in both modulators and altering the AWG delay of channel 2 (going to modulator 2) until the maximum extinction ratio is achieved. This was repeated for each RF tone and the recorded optimum delays were applied to the corresponding tones in the final waveform (see Supplement 1, sect B) to get maximized ER for all three tones simultaneously. For the single tone, an ER greater than 20 dB was achieved, while for the three-tone scenario, an 18 dB ER was observed at the coherent combined output. This represents a delay mismatch around 10 ps which is equivalent to a phase mismatch of $\simeq 6$ degrees according to Eq. (7) and (8).

This calibration shows that the pump-phase modulation between two modulators can be matched well. Going from the coherent combining setup (Fig. 3(a)) to the PSA (Fig. 3(b)) is straightforward as the PSA gain is also proportional to the locking efficiency η in (5) [23]. Here, an equivalent extinction ratio as for the coherent combining is obtained from the ratio of the power P_s (e.g. measured using a power meter) between phase-sensitive gain and phase-sensitive attenuation in the PSA (switched using the PLL). In principle, the exact same magnitude transfer and delay characterization we discussed for the coherent combining technique can be performed using the phase-sensitive aspect of the PSA. However, since the quality of the characterization depends on the gain in this case and the gain is severely limited by SBS when only applying one RF tone at a time, coherent combining is a better option for obtaining close to optimal voltages and delays. Applying these initial optimum values in the PSA setup and adjusting the delay between the two modulators (between AWG channels), to account for the different optical path lengths in the setups of Fig. 3(a,b), a close to maximized ER was achieved. Some further fine-tuning of the individual delays and amplitudes enabled us to achieve an ER of approximately 15 dB with all three RF tones applied and with an achieved SBS power threshold increase of 12.6 dB. From Eqs. (7) and (8), we observe that small variations in the counter-phase mismatch ($\Delta\phi$) can significantly impact $\langle\eta\rangle$. As reflected in Eq. (6), these changes affect $\langle ER\rangle$ in our measurements. Additionally, introducing a nonlinear element like a PSA, operating in the gain regime, can amplify such variations.

To visualize the idler spectral broadening during this optimization process (as a complement to monitoring ER during fine-tuning), we used the delayed self-heterodyne detection (DSHD) method. This method is explained further in sections B and C in Supplement 1.

2.3. Residual pump-phase penalty

Any uncompensated phase mismatches will negatively impact the performance of the PSA. These phase mismatches limit the locking efficiency (η), as described in Eq. (5) from which the noise figure penalty (F_η) of the PSA and the bit-error ratio (BER) [22,23] are given by

$$\mathrm{F}_\eta(\Delta\phi) = \frac{1}{\eta} \tag{9}$$

and

$$\mathrm{BER} = \frac{1}{2}\mathrm{erfc}\left\{\sqrt{\mathrm{SNR}}\right\}, \quad \mathrm{SNR} \propto \frac{1}{F_\eta} \tag{10}$$

respectively. Therefore, minimizing uncompensated phase mismatches will significantly enhance the performance of the dual-pump FOPA.

Optics EXPRESS

In terms of idler broadening, the expression $2\langle\eta\rangle - 1 \approx \exp(-\Delta\phi^2/4)$ represents the non-broadened fraction of power in the idler whereas $2(1 - \langle\eta\rangle)$ is the fraction of power redistributed on a wider spectrum. No simple metric is developed for estimating the idler spectral broadening width, it is instead visualized using the delayed-self-heterodyne technique.

3. Performance of the residual pump phase-minimization

Here we investigate the idler spectral broadening using delayed-self heterodyne techniques and BER measurement of a communication signal to evaluate the performance of our pump-phase minimization technique in the context of wavelength conversion and low-noise amplification.

3.1. Experimental setup

The experimental setup is depicted in Fig. 4. A continuous wave (CW) optical signal was used for initial optimization and investigation. For BER-analysis, a $2^{15} - 1$ bit long pseudo-random bit sequence-pattern (PRBS) pattern was used to modulate the CW signal at a symbol rate of 10 Gbaud binary phase shift keying (BPSK) in the external IQ-modulator.

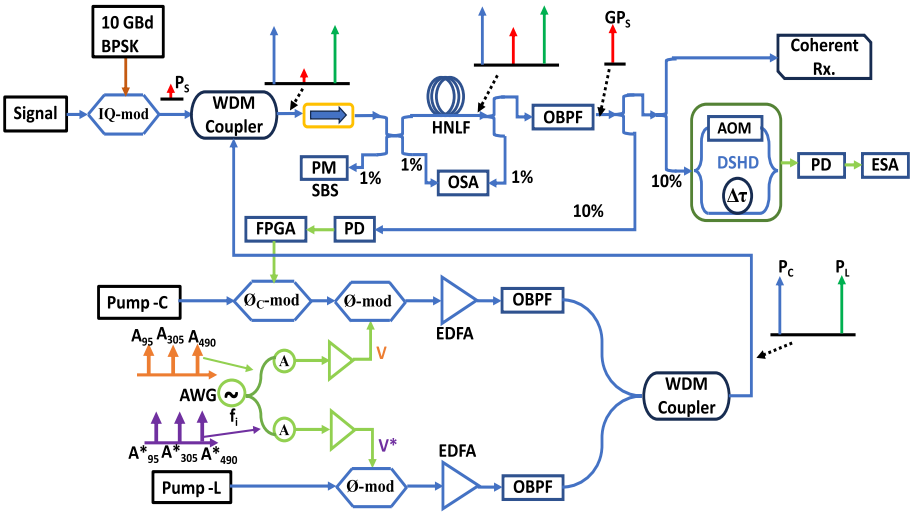

Fig. 4. Schematic of the PSA-setup. Polarization controllers were used to align the polarization of all waves at all points. WDM, wavelength-division multiplexer; OBPF, optical band-pass filter; PM, power meter; PD, photo-detector; FPGA, field programmable gate array. ϕ-mod /ϕ_c-mod, electro-optic phase modulator, ESA, electrical spectrum analyser, Δt, fiber delay, AOM, Acoustic optic modulator.

The two phase-modulated pumps (for SBS suppression) at 1536.6 nm and 1587.1 nm were separately amplified using high-power C- and L-band EDFAs, optically filtered to reduce any out-of-band ASE, thus increasing the optical signal-to-noise ratio (OSNR) of the pumps and reducing the impact of ASE in the FWM process [28,29]. The pumps were then combined through a WDM, resulting in a total pump power of 30.1 dBm (27.1 dBm per pump). The pumps and the received signal (1561.45 nm, (P_s)) were combined in another WDM before entering the phase-sensitive amplification stage. In this configuration, the pumps amplified in a 350 m long HNLF with zero dispersion wavelength (λ_0) at 1561.7 nm and an effective nonlinear coefficient (γ) of 25 $W^{-1}km^{-1}$.

A 1% tap was used at the HNLF input in the reverse direction to measure the back-scattered optical power using a power meter. Another 1% tap at the HNLF output was connected to an optical spectrum analyzer (OSA) to capture the amplified spectrum (Fig. 5), from which the

Optics EXPRESS

parametric gain and optical NF were estimated. The left and right insets of Fig. 5 compare the measured HNLF output signal power with the phase-locked and free-running BPSK signal and CW signal respectively at the PSA output, showing the expected 3 dB gain increase from phase-locking.

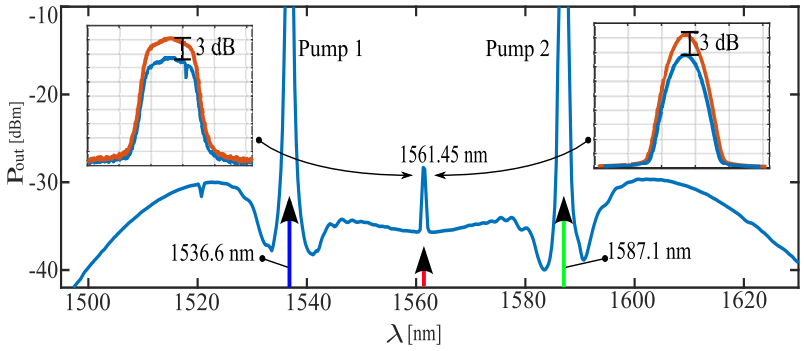

Fig. 5. Measured PSA-HNLF optical output spectrum with 0.5 nm resolution. Insets show the unlocked (blue) vs. phase-locked (orange) amplified BPSK signal to the left and CW signal to the right.

The amplified signal at the 99%-port was filtered out, with a 10% tap output directed to a photodetector (PD) and the optical phase-locked loop (OPLL). The optical phase error signal generated was used to keep the PSA phase-locked by controlling the phase of ϕ_c-mod. The same low-noise laser (linewidth of ~ 100 Hz) was used to generate both signal and pump waves [25,30], thus removing any phase-locking penalty due to uncorrelated waves (which would be present in a practical system). The purpose of the OPLL was thus only to compensate for the natural phase drifts between the signal and pumps. We investigate in [25] the realistic case with locking of uncorrelated waves.

The other (90%-) port was further tapped, with 10% of the signal directed for idler broadening measurement using the DSHD and ESA arrangement. The final output was used for bit error rate (BER) measurements. We observed that once the amplitude and delay (phase) of the pump modulation tones (m = 1, 2, 3) were adjusted, they remained very stable. Over extended hours, we did not detect any significant variations in the idler spectrum, even when using the DSHD setup for hours. Also, this stability was observed in the PSA output at the OSA and during the BER measurements. However, slow polarization drifts must be compensated by aligning the polarization of the waves continuously to get correct ER measurement.

For BER measurements, the preamplified signal was bandpass filtered and mixed with a local oscillator (LO) with a 1 MHz linewidth in an intradyne coherent receiver [31–33]. To minimize noise in digital filtering [34] and improve the signal-to-noise ratio (SNR) [34,35], care was taken to match the LO wavelength to the signal wavelength. For each received power level, batches of 500,000 symbols were captured using a real-time scope and processed offline using digital signal processing (DSP) [36] based on QAMpy [37]. The DSP involved resampling, IQ imbalance and frequency offset compensation, constant modulus, and carrier phase estimation, as described in [36]. For BPSK, the constant modulus equalizer filter taps were calculated using a generated digital copy of the received signal, consisting of the sampled signal plus a delayed and 90-degree rotated copy of the signal. This method replicated QPSK and made it function with the constant-modulus equalizer.

Optics EXPRESS

3.2. Idler broadening suppression

Since we implemented the degenerate signal-idler scenario, measuring the signal spectral width using the DSHD system gives the effect of pump-phase modulation on the idler. Therefore the signal spectral broadening was measured using the DSHD method and observed through an electrical spectrum analyzer (ESA), as shown in Fig. 4 (a detailed view is in Fig. S4(a) & S7 in Supplement 1). This method provides high sensitivity and resolution for measuring linewidth. More details about the method can be found in [24]. Unlike the method used in [2,17], which requires a high-precision narrow linewidth local oscillator (LO) laser and precise matching of the LO and idler phase and wavelength, the DSHD method avoids many of these issues by using the same signal power-divided and self-reference in a Mach-Zehnder interferometer.

The PSA output signal was filtered and analyzed using the DSHD setup and the ESA for optimum out-of-phase delay between the pump phases. Figure 6 shows the ESA traces captured for optimum phase alignment between two pumps as discussed in Section 2. Only a single tone should appear at the AOM frequency when the pumps are perfectly modulated counter-phase [17] (refer to section C in Supplement 1). However, by closely examining the ESA view over and adjusting the resolution bandwidth (Fig. 6(d)), some residual side tones were identified after our optimization. The maximum suppression achieved between the main tone (contributing from the self-heterodyne components) and the highest side tone (contributing from the cross-heterodyne components) was around 30 dB (in the electrical domain) which matches the measured PSA extinction ratio of 15 dB (in the optical domain) squared. No side tones were visible beyond 0.6 GHz for the optimised phase values, indicating that significant phase matching of the pump modulation phases was achieved, as compared to [17].

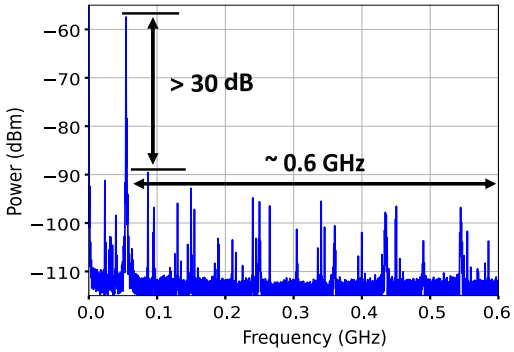

Fig. 6. DSHD Idler spectra obtained at the ESA for 2 MHz of resolution bandwidth (RBW) and 10 kHz of video bandwidth (VBW)

Figure 7 presents the ESA traces for different phase mismatches introduced via a delay (equivalent to τ_e in Eq. (7) for all tones) between the RF signals driving the modulators. Sixteen different delay values were tested (Table S2 in Supplement 1), but only six representative delay values are displayed here to illustrate the DSHD spectra, ranging from optimal to worse phase alignments. In the worst depicted case (Fig. 7(f)), the power of the side tones are higher than the main tone, with significant spectral broadening up to 2.4 GHz. However, the sideband spread was reduced from 2.4 GHz to 0.6 GHz under optimal conditions. Comparing Fig. 7(a) and (f) confirms the success of optimizing pump phases to achieve out-of-phase modulation while minimizing component mismatches and residual amplitude modulation.

3.3. BER and NF measurement

A more comprehensive analysis was conducted by measuring the bit-error ratio for the 10 Gbaud BPSK signal to characterize the performance degradation from idler spectral broadening. The

Optics EXPRESS

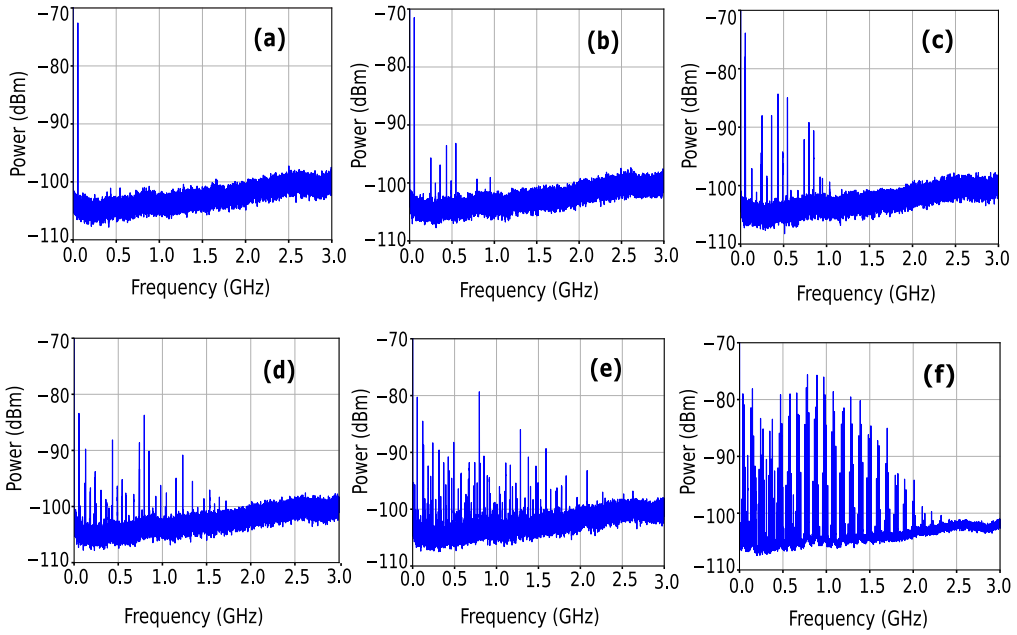

Fig. 7. DSHD Idler spectra for CW signal input. (a)–(f) are for the analog delay difference values (τ) of 0ps (optimum), 60ps, 120ps, 180ps, 300ps, 480ps respectively), all traces were obtained for 2 MHz of RBW and 10 kHz of VBW.

BER values as a function of received signal power were measured as shown in Fig. 8. The experimental curves show the averages from the M best-performing batches out of N total batches, where M/N = 10/20. Some batches were affected by sporadic DSP divergences and intermittent phase jumps of 2π in the control modulator (ϕ-mod) as seen in Fig. 4. Therefore, averaging using the M/N ratio offers a more accurate description of the true BER performance [25].

The PSA BPSK performance was evaluated for sixteen different analog time delays between two pumps from 0 ps to 380 ps (Table S2 in Supplement 1 text), however, only eight selected delays are plotted in Fig. 8. The BER for larger delays were not measured as the extinction ratio was reaching zero and the OPLL was not responding. The selections were made to depict the minimum, medium and largest BER matches as the pump phases were misaligned from optimum. In Fig. 8 the PSA performance at the best delay closely matches with the theoretical 1.25 dB NF curve.

The uncertainty in NF measurements is estimated at 0.1 dB, attributed to the precision of the power meters used for calibrating the PSA's input and output power monitor ports. The NF penalty was calculated to be 0.05 dB due to limited HNLF gain necessitating the EDFA in front of the receiver, 0.2 dB from pump phase modulation for SBS suppression [25]. As a result, the final PSA NF, accounting for all penalties, is 1.45 ± 0.1 dB for the BPSK signal at the optimal pump phase difference when compared with the theoretical NF curve (Fig. 8).

Theoretical and simulation (at 180 ps) BER curves were generated using Eq. (10). Theoritical BER was calculated based on SNR values, assuming NF values as shown in Fig. 8. For simulations at 180 ps delay mismatch, the η value was determined using Eq. (8), and the NF value was subsequently calculated as F_0/η, with F_0 set to 1.25 dB. Using this NF value, the corresponding SNR was derived, and BER was then estimated.

It can be seen that the system gets more prone to errors as the delay increases. At 180 ps delay, the system experiences a significant outage and we can see from the DSHD spectrum (Fig. 7(d)) that the difference between the main tone and the next dominant tone is almost 0 dB. This will

Optics EXPRESS

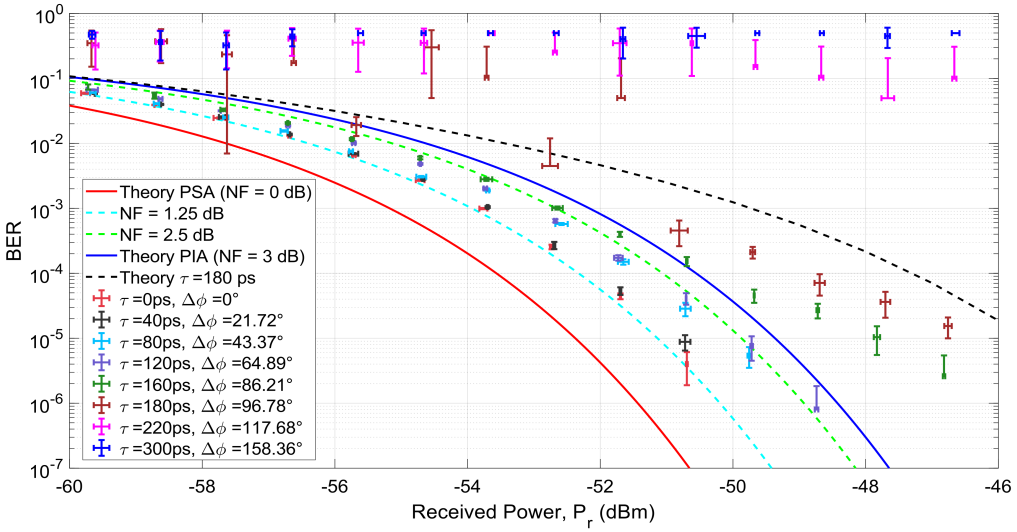

Fig. 8. BER vs. received power for the BPSK-signal for some selected delays (with a corresponding phase difference ($\Delta\phi$) calculated using Eq. (8)) between the pumps with standard deviation error bars. Theoretical BER curves for different NFs are included for comparison. $\tau = 0$ represents the optimum case.

impact the locking of the OPLL which may lock to the incorrect tone. This we can see from the BER curve for all $\tau_e \geq 180$ ps.

4. Conclusion

We evaluated the performance of a degenerate dual-pump phase-sensitive amplifier (PSA) using counter-phased RF tones to suppress stimulated Brillouin scattering (SBS). By applying phase modulation to both pumps and employing coherent combining, we minimized residual pump-phase modulation, analyzed phase cancellation through extinction ratio measurements, and reduced frequency-dependent RF component effects. This streamlined optimization of balanced modulation depths and ideal phase mismatch at the FOPA input.

We used delayed self-heterodyne detection (DSHD) to analyze the idler, providing a direct alternative to homodyne methods. DSHD measured pump-phase cancellation in the idler. The pump phase optimization enabled the reduction of residual modulation bandwidth about 0.6 GHz with optimal phase alignment and suppressing cross-heterodyne components by over 30 dB. Coherent combining quantified RF mismatches, while fine-tuning the modulation signal's delay compensated for optical path length mismatches, simplifying the process.

By characterizing the transfer function of the applied phase modulation, we achieved precise phase-matching between pumps, ensuring FOPA performance with a maximum NF penalty of only 0.2 dB [25]. The reduction in idler spectral broadening facilitates the implementation of low-noise dual-pump PSAs and paves the way for a wide range of applications. These results demonstrate that the idler can match the signal in quality, highlighting the approach's potential for practical applications in fibre-based OPAs, including phase-sensitive amplification and wavelength conversion systems [2,5,13,38–40].

Funding. Vetenskapsrådet (VR-2015-00535).

Optics EXPRESS

Acknowledgments. We extend our gratitude to Z. He for assistance with BPSK implementation, K. Vijayan and P. Zhao for insightful discussions on PSA experiments, M. Karlsson for valuable input on phase erasure techniques, J. Schröder for discussions on digital signal processing for BPSK, and C. Skehan, M. Jamshidifar for support in the lab.

Disclosures. The authors declare that there are no conflicts of interest related to this article.

Data availability. Data underlying the results presented in this paper are available in Ref. [41].

Supplemental document. See Supplement 1 for supporting content.

References

1. G. P. Agrawal, *Nonlinear Fiber Optics* (Academic Press Inc., 2019), 6th ed.
2. M. E. Marhic, *Fiber Optical Parametric Amplifiers, Oscillators and Related Devices* (Cambridge University Press, 2007).
3. S. J. B. Yoo, "Wavelength conversion technologies for WDM network applications," J. Lightwave Technol. **14**(6), 955–966 (1996).
4. A. E. Willner, M. C. Cardakli, O. H. Adamczyk, *et al.*, "Key building blocks for all-optical networks," IEICE Trans. Commun. **E83-B**, 2166–2177 (2000).
5. K. E. Stubkjaer, A. Klock, P. B. Hansen, *et al.*, "Wavelength converter technology," IEICE Trans. Commun. **E82-B**, 390–400 (1999).
6. I. Brener, B. Mikkelsen, G. Raybon, *et al.*, "160 Gbit/s wavelength shifting and phase conjugation using periodically poled LiNbO3 waveguide parametric converter," Electron. Lett. **36**(21), 1788–1790 (2000).
7. S. Watanabe, S. Takeda, and T. Chikama, "Interband wavelength conversion of 320 Gb/s (32 × 10 Gb/s) WDM signal using a polarization-insensitive fiber four-wave mixer," in *Proc. ECOC*, vol. 3 (1998), pp. 83–87.
8. O. Aso, S. Arai, T. Yagi, *et al.*, "Broadband four-wave mixing generation in short optical fibers," Electron. Lett. **36**(8), 709–711 (2000).
9. J. M. C. Boggio, C. Lundström, J. Yang, *et al.*, "Double-pumped FOPA with 40 dB flat gain over 81 nm bandwidth," in *ECOC* (2008), pp. 21–25.
10. M.-C. Ho, K. Uesaka, M. E. Marhic, *et al.*, "200-nm-bandwidth fiber optical amplifier combining parametric and Raman gain," J. Lightwave Technol. **19**(7), 977–981 (2001).
11. J. Hansryd and P. A. Andrekson, "Broadband CW pumped fiber optical parametric amplifier with 49 dB gain and wavelength conversion efficiency," in *Proc. OFC* (2000), paper PD3–1.
12. S. Radic, "Parametric amplification and processing in optical fibers," Laser Photonics Rev. **2**(6), 498–513 (2008).
13. P. A. Andrekson and M. Karlsson, "Fiber-based phase-sensitive optical amplifiers and their applications," Adv. Opt. Photonics **12**(2), 367–428 (2020).
14. R. Slavík, F. Parmigiani, J. Kakande, *et al.*, "All-optical phase and amplitude regenerator for next-generation 384 telecommunications systems," Nat. Photonics **4**(10), 690–695 (2010).
15. M. Bastamova, V. Gordienko, N. Doran, *et al.*, "Impact of pump phase modulation on QAM signals in polarization-insensitive fiber optical parametric amplifiers," Opt. Fiber Technol. **84**, 103758 (2024).
16. F. S. Yang, M. E. Marhic, and L. G. Kazovsky, "CW fiber optical parametric amplifier with net gain and wavelength conversion efficiency greater than one," Electron. Lett. **32**(25), 2336–2338 (1996).
17. M.-C. Ho, F. S. Yang, M. E. Marhic, *et al.*, "Idler spectral broadening suppression in two-pump optical parametric amplifier," Proc. SPIE **3749**, 96–97 (1999).
18. S. Yamashita and K. Torii, "Highly efficient optical fiber wavelength conversion without spectral spread," in *Proc. OECC* (2000), pp. PD2–PD8.
19. T. Umeki, M. Asobe, and H. Takenouchi, "In-line phase sensitive amplifier based on PPLN waveguides," Opt. Express **21**(10), 12077–12084 (2013).
20. K. J. Lee, F. Parmigiani, S. Liu, *et al.*, "Phase sensitive amplification based on quadratic cascading in a periodically poled lithium niobate waveguide," Opt. Express **17**(22), 20393–20400 (2009).
21. Z. Yan, H. He, H. Liu, *et al.*, "χ2-based AlGaAs phase sensitive amplifier with record gain, noise, and sensitivity," Optica **9**(1), 56 (2022).
22. R. Larsson, J. Schröder, M. Karlsson, *et al.*, "Coherent combining of low-power optical signals based on optically amplified error feedback," Opt. Express **30**(11), 19441–19455 (2022).
23. R. Larsson, K. Vijayan, J. Schröder, *et al.*, "Low-noise phase-sensitive optical parametric amplifier with lossless local pump generation using a digital dither optical phase-locked loop," in *Optical Fiber Communications Conference and Exhibition* (2023), pp. 1–3.
24. D. J. Derickson, *Fiber Optic Test and Measurement* (Prentice Hall, 1998), 1st ed.
25. R. Larsson, R. U. Weerasuriya, and P. A. Andrekson, "Ultralow-noise preamplified optical receiver using conventional single-wavelength transmission," Optica **11**(11), 1497–1502 (2024).
26. J. Coles, "Advanced phase modulation techniques for stimulated Brillouin scattering suppression in fiber optic parametric amplifiers," Ph.D. thesis, UC San Diego (2009).
27. R. Larsson, K. Vijayan, J. Schröder, *et al.*, "Supplementary document for Low-Noise Phase-Sensitive Optical Parametric Amplifier with Lossless Local Pump Generation using a Digital Dither Optical Phase-Locked Loop," (Optica Publishing Group, 2023).
28. E. Desurvire, *Erbium-Doped Fiber Amplifiers: Principles and Applications* (Wiley-Interscience, 1994), 1st ed.

Optics EXPRESS

29. S. Alahakoon, D. Munasinghe, G. S. Samarakkody, *et al.*, "OSNR and dispersion tolerance of FWM based optical carrier recovery scheme," J. Phys. Commun. **4**(9), 095004 (2020).
30. R. Larsson, R. Weerasuriya, and P. Andrekson, "Supplementary document for Ultralow noise preamplified optical receiver using conventional single wavelength transmission," (2024).
31. S. J. Savory, "Digital Coherent Optical Receivers: Algorithms and Subsystems," IEEE J. Sel. Top. Quantum Electron. **16**(5), 1164–1179 (2010).
32. B. Spinnler, "Equalizer Design and Complexity for Digital Coherent Receivers," IEEE J. Sel. Top. Quantum Electron. **16**(5), 1180–1192 (2010).
33. A. Leven, N. Kaneda, and S. Corteselli, "Real-time implementation of digital signal processing for coherent optical digital communication systems," IEEE J. Sel. Top. Quantum Electron. **16**(5), 1227–1234 (2010).
34. E. Ip, A. P. T. Lau, D. J. F. Barros, *et al.*, "Coherent detection in optical fiber systems," Opt. Express **16**(2), 753–791 (2008).
35. N. Antoniades, G. Ellinas, and I. Roudas, *WDM systems and networks: Modeling, simulation, design and engineering* (Springer, 2012).
36. S. J. Savory, "Digital filters for coherent optical receivers," Opt. Express **16**(2), 804–817 (2008).
37. J. Schröder, M. Mazur, and M. Brehler, "Chalmersphotonicslab/qampy: v0.2," https://github.com/chalmersphotonicslab/qampy (2019).
38. R. Kakarla, J. Schröder, and P. A. Andrekson, "One photon-per-bit receiver using near-noiseless phase-sensitive amplification," Light: Sci. Appl. **9**(1), 153 (2020).
39. M. Butt, G. Voronkov, E. Grakhova, *et al.*, "Environmental Monitoring: A Comprehensive Review on Optical Waveguide and Fiber-Based Sensors," Biosensors **12**(11), 1038 (2022).
40. F. Hudelist, J. Kong, C. Liu, *et al.*, "Quantum Metrology with Parametric Amplifier-Based Photon Correlation Interferometers," Nat. Commun. **5**(1), 3049 (2014).
41. R. U. Weerasuriya, R. Larsson, and P. A. Andrekson, "Effect of counter-phase pump modulation of phase-sensitive amplifiers noise performance and sbs suppression," Zenodo (2025), https://doi.org/10.5281/zenodo.14779698.